RAMANUJAN SUMS FOR IMAGE PATTERN ANALYSIS

GUANGYI CHEN

Department of Computer Science and Software Engineering, Concordia University, 1455 de Maisonneuve West, Montreal, Quebec, Canada H3G 1M8.

guang_c@cse.concordia.ca

SRIDHAR KRISHNAN

Department of Electrical and Computer Engineering, Ryerson University, Toronto, Ontario, Canada M5B 2K3.

krishnan@ee.ryerson.ca

TIEN D. BUI

Department of Computer Science and Software Engineering, Concordia University, 1455 de Maisonneuve West, Montreal, Quebec, Canada H3G 1M8.

bui@cse.concordia.ca

Ramanujan sums (RS) have been found to be very successful in signal processing recently. However, as far as we know, the RS have not been applied to image analysis. In this paper, we propose two novel algorithms for image analysis, including moment invariants and pattern recognition. Our algorithms are invariant to the translation, rotation and scaling of the 2D shapes. The RS are robust to Gaussian white noise and occlusion as well. Our algorithms compare favourably to the dual-tree complex wavelet (DTCWT) moments and the Zernike's moments in terms of correct classification rates for three well-known shape datasets.

Keywords: Ramanujan Sums (RS); invariant features; moment invariants; pattern recognition; Fourier transform (FT); Gaussian white noise; occlusion.

AMS Subject Classification: 68T10, 91C20, 62H35

1. Introduction

The Ramanujan Sums (RS) [9] were proposed by R. Ramanujan in 1918. However, only recently they were introduced to signal processing ([12, 8, 10, 6, 7]). The RS are orthogonal in nature and therefore offer excellent energy conservation, similar to the Fourier transform (FT). The RS are operated on integers and hence can obtain a reduced quantization error implementation. Even though the RS have such important properties, they have not been applied to image analysis such as moment invariants, shape recognition, and noise robustness.

In this paper, we propose two novel algorithms for image analysis, including moment invariants and shape recognition. Our algorithms are invariant to the

translation, rotation, and scaling of the input 2D shapes. Our experiments show that our proposed algorithms compare favourably to the dual-tree complex wavelet (DTCWT) moments and the Zernike's moments for classifying three well-known shape datasets.

The organization of the paper is as follows. Section 2 reviews the RS transform. Section 3 proposes the RS moments for pattern recognition. Section 4 develops a shape recognition algorithm by using the RS function. Section 5 studies the noise robust property of the RS transform. Section 6 conducts some experiments in order to compare our proposed algorithms with existing algorithms. Finally, Section 7 draws the conclusions of this paper.

2. Ramanujan Sums (RS)

The RS are the m^{th} powers of q^{th} primitive roots of unity, defined as

$$c_q(m) = \sum_{p=1;(p,q)=1}^{q} \exp(2i\pi\frac{p}{q}m)$$

where (p,q) =1 means that the greatest common divisor (GCD) is unity, i.e., p and q are co-primes. An alternate computation of RS can be given as

$$c_q(m) = \mu(\frac{q}{(q,m)})\frac{\phi(q)}{\phi(\frac{q}{(q,m)})}$$

Let $q = \prod_i q_i^{\alpha_i}$ (q_i prime). Then, we have

$$\phi(q) = q\prod_i(1-\frac{1}{q_i}).$$

The Mobius function $\mu(m)$ is defined as

$$\mu(m) = \begin{cases} 0, \, if\, m\, contains\, a\, square\, number \\ 1, \, if\, m = 1 \\ (-1)^k, \, if\, m\, is\, a\, product\, of\, k\, prime\, numbers. \end{cases}$$

The first few values of $c_q(m)$are given as follows:

$$c_1 =< 1 >, c_2 =< -1, 1 >, c_3 =< -1, -1, 2 >, c_4 =< 0, -2, 0, 2 >, ...$$

where <> indicates the period. For example, $c_4(1)$=0, $c_4(2) = -2$, $c_4(3) = 0$, $c_4(4) = 2$, $c_4(5) = 0$, $c_4(6) = -2$, etc. We give Table 1 for $c_q(n)$ in range q∈[1,20] here.

The RS has the following multiplicative property:

$$c_{qq'}(n) = c_q(n)c_{q'}(n) \text{ if (q,q')=1}$$

and also the orthogonal property:

$$\sum_{n=1}^{qq'} c_q(n)c_{q'}(n) = 0 \text{if q}\neq\text{q'}.$$

$$\sum_{n=1}^{q} c_q^2(n) = q\phi(q) \text{otherwise}.$$

The 1D RS transform of a signal *x(m)* with M samples is defined as

$$x_q = \frac{1}{\phi(q)}\frac{1}{M}\sum_{m=1}^{M} x(m)c_q(m)$$

In this paper, we study the applications of RS for image analysis, including moment invariants, shape recognition, and noise robustness. We find out that our proposed algorithms compare favourably to the DTCWT moments [3] and the Zernike's moments [5]. In addition, the RS are robust to Gaussian white noise. In order to speed up the calculation, we precompute $c_q(m)$only once and save them into a file for later retrieval. This can save a lot of computation time.

3. RS Moment Invariants

In this section, we propose a set of new moments based on the RS. Let $f(x, y)$ represent a 2D binary image object in the (x,y)-coordinate and its corresponding form in the polar coordinate be $f(r, \theta)$, where $r \in [0, 1]$ and $\theta \in [0, 2\pi)$. The relationship between $f(x, y)$ and $f(r, \theta)$ is given as follows:

$$x = r\cos(\theta),$$

$$y = r\sin(\theta).$$

Let the RS function sweep across in all angular rotations in the moment calculation; it will be able to extract either global or local information depending on the values of q and k. We can then introduce a set of moment invariants by using RS functions, defined as:

$$A_{q,k} = |\int_0^{2\pi}\int_0^1 f(r,\theta)c_q(n_r)e^{-ik\theta}rdrd\theta|$$

where $n_r = \lfloor r \times N + 0.5 \rfloor$ and N is the number of rows in the image f. Note that in the above equation, we need to discretize the image f in the polar coordinate system (r,θ). For ease of notation, we still write the r and θ as continuous variables. It is well known that higher-order moments are too sensitive to Gaussian white noise; they cannot be used as the discriminative features of an object. This is also true for the proposed RS moment invariants in this paper. It is easy to show that the proposed RS moments are invariant to the rotation of the 2D pattern images, which is very useful in invariant pattern recognition. This is because

$$\begin{aligned}
&|\int_0^{2\pi}\int_0^1 f(r,\theta+\theta_0)c_q(n_r)e^{-ik\theta}rdrd\theta| \\
&= |\int_0^{2\pi}\int_0^1 f(r,\theta)c_q(n_r)e^{-ik\theta}rdrd\theta| \times |e^{ik\theta_0}| \\
&= |\int_0^{2\pi}\int_0^1 f(r,\theta)c_q(n_r)e^{-ik\theta}rdrd\theta|
\end{aligned}$$

The Zernike's moments [5] can be used to extract rotation invariant features from the input image. Let

$$V_{pq} = R_{pq}(r)\exp(jq\theta),$$

where $r = \sqrt{x^2+y^2}$is the length of the vector from the origin to the pixel *(x,y)* and $\theta = \arctan(y/x)$. Also,

$$R_{pq}(r) = \sum_{l=0}^{(p-|q|)/2} (-1)^l \frac{(p-l)!}{l!(\frac{p+|q|}{2}-l)!(\frac{p-|q|}{2}-l)!} r^{p-2l}$$

Now, let us define the Zernike moment of order p with repetition q as

$$Z_{pq} = \iint f(x,y)V_{pq}^*(x,y)dxdy.$$

Since the Zernike's moments are very complex to compute, they should be slower than RS moments. In this paper, we calculate $c_q(n_r)$only once and save them into a file for later retrieval.

The major contribution of this algorithm is the following. We have proposed a new set of moment invariants by using the RS. This set of RS moments is invariant to the rotation of the 2D patterns, which is very important for invariant pattern recognition. Experimental results show that the proposed RS moment invariants compare favourably to the Zernike's moments and the DTCWT moments for recognizing 2D shapes in the first shape dataset. However, the RS moments are not as good as the Zernike's moments and the DTCWT moments for the second shape dataset. The RS moments are better than the Zernike's moments for the third shape dataset.

Note that the RS moments introduced in this paper can also be called as radial moments. Radial moments are a well-known tool for object recognition. Their kernel functions all have the form similar to our formula, where there is always a harmonic function in angular direction and (usually orthogonal) polynomials in a radial direction. Thanks to the Fourier-shift theorem applied in angular direction, all radial moments preserve their magnitude under arbitrary rotation. Individual radial moments differ from each other namely by the radial function used, each of them having its pros and cons [4].

4. Shape Recognition

Invariance in terms of translation, rotation and scale is a very important aspect in 2D shape recognition. For translation invariance, we can move the centroid of the 2D shape to the centre of the shape image. For scaling invariance, we can use a standard normalization technique given in [2], For example, the scaling factor of a black-and-white image *f(x,y)* is given as

$$\alpha = \sqrt{\frac{\beta}{\sum_{x,y} f(x,y)}}.$$

where β is a constant. In this paper, we have chosen β=1500, 3000 and 5000 for the first, second and third dataset, respectively. We propose to perform the Radon transform to the input 2D shape *f(x,y)* [1]:

$$R(r,\theta) = \int_x \int_y f(x,y)\delta(r - x\cos\ \theta - y\sin\ \theta)\ dxdy$$

where $\delta()$ is the Dirac delta function. In this way, the rotation of the 2D shape is converted to circular shift in θ. For every fixed θ , we can perform the convolution between *R(r,θ)* and $c_q(1:q)$, *q∈[1,Q],* along the r direction:

$$B(\theta,q) = conv(R(r,\theta), fliplr(c_q(1:q)))$$

where *fliplr()* is a function to flip its filter and *conv()* is the convolution operation. Let us circularly pad q elements after the vector *B(θ,q),* and we obtain$\hat{B}(\theta,q)$. Now, convert the vector$\hat{B}(\theta,q)$into a matrix with q columns by the Matlab command:

$$D^q(q_i,\theta) = vec2mat(\hat{B}(\theta,q),q).$$

Next, take the sum along each column of $D^q(q_i,\theta\ )$*:*

$$SD(q,\theta) = \sum_{q_i} D^q(q_i,\theta).$$

Also,

$$r(q^*,\theta) = \max_q(|SD(q,\theta)|/\phi(q))$$

Finally, we can take the sum along the θ direction so that we can obtain the rotation invariant features $F(q*) = \sum_\theta r(q*,\theta)$ for *q*∈[1,Q],*

The computational complexity of this algorithm can be given as follows. For an $M\times N$ image, the Radon transform takes $O(MN\ \log(MN))$flops of operation. The RS transform for each row of *R(r,θ)* takes $O(N\ \log(N))$ operations. Since we have M rows in total, the RS for the image *R(r,θ)* is $O(MN\ \log(N))$ operations. Therefore, the total computational complexity of our proposed method in this paper is $O(MN\ (\log(MN) + \log(N)) = O(MN\ \log(MN^2))$.

The major contributions of this algorithm are the following. We are the first who have successfully applied the RS to shape recognition. Our proposed method is invariant to the translation, rotation, and scaling of the input shapes. Our experimental results show that our proposed algorithm outperforms both the DTCWT moments and the Zernike's moments in terms of correct classification rates for the first and the second shape datasets. For the third dataset, out RS algorithm is not as good as the DTCWT moments, but it is much better than the Zernike's moments. In addition, we have proposed to precompute the RS basis function $c_q(m)$offline and save them into a file, and then retrieve them during the calculation without computing them online. This can save a huge amount of computation time.

5. Noise Robustness

We now discuss the reasons why the RS are more noise robust than the FT. Let the noise-free signal be $x(i)$and the noisy signal be

$$y(i) = x(i) + \sigma_n z(i),$$

where σ_n is the standard deviation of the noise and $z(i)$is the noise with Gaussian distribution *N(0,1)*. We know that

$$c_1 =< 1 >, c_2 =< -1, 1 >, c_3 =< -1, -1, 2 >, c_4 =< 0, -2, 0, 2 >, ...$$

Since the RS coefficients can be calculated as follows:

$$r_q = \frac{1}{\phi(q)} \times \frac{1}{M} \sum_{i=1}^{M} x(i) c_q(i)$$

Therefore, when *q=1*, we have

$$\begin{aligned} & r_1^* = \tfrac{1}{\phi(1)} \times \tfrac{1}{M} \textstyle\sum_{i=1}^{M} y(i) c_1(i) \\ & = \tfrac{1}{\phi(1)} \times \tfrac{1}{M} (\textstyle\sum_{i=1}^{M} x(i) c_1(i) + \sigma_n \sum_{i=1}^{M} z(i) c_1(i)) . \\ & = \tfrac{1}{M} \textstyle\sum_{i=1}^{M} x(i) = r_1 \end{aligned}$$

This is because$c_1 =< 1 >$and $\sum_{i=1}^{M} z(i) = 0$. This means that the Gaussian white noise does not affect the RS coefficient r_1. When *q=2*, we have

$$\begin{aligned} & r_2^* = \tfrac{1}{\phi(2)} \times \tfrac{1}{M} \textstyle\sum_{i=1}^{M} y(i) c_2(i) \\ & = \tfrac{1}{\phi(2)} \times \tfrac{1}{M} (\textstyle\sum_{i=1}^{M} x(i) c_2(i) + \sigma_n \sum_{i=1}^{M} z(i) c_2(i)) \\ & = r_2 + \sigma_n \tfrac{1}{\phi(2)} \times \tfrac{1}{M} \textstyle\sum_{i=1}^{M/2} (z(2i) - z(2i-1)) \\ & = r_2 + \sigma_n \tfrac{1}{\phi(2)} \times \tfrac{1}{M} (\textstyle\sum_{i=1}^{M/2} z(2i) - \sum_{i=1}^{M/2} z(2i-1)) \\ & \approx r_2 \end{aligned}$$

This is because $c_2 =< -1, 1 >$ and $\sum_{i=1}^{M/2} z(2i) = 0$ and $\sum_{i=1}^{M/2} z(2i-1) = 0$. Similarly, we can derive other RS coefficients so that $r_q^* \approx r_q$for $q>2$.

6. Experimental Results

We conducted experiments for three shape datasets. The first dataset [13] is a subset of the MPEG-7 CE Shape-1 Part-B data set, which has 216 shapes in total. This dataset has 18 categories with 12 shapes in each category. The dataset is shown in Fig. 1. Each shape is matched against every other shape in the dataset. As there are 12 shapes in each category, up to 12 nearest neighbours are from the same category. We rate the performance based on the number of times the 12 nearest neighbours are in the same category. The shape classes are very distinct, but the data set shows substantial within-class variations.

The second dataset [13] in our experiments is the fighter airplane shape dataset, which includes Mirage, Eurofighter, F-14, Harrier, F-22 and F-15. Since F-14 has

two possible shapes, one when its wings are closed and another when its wings are opened, total number of shape classes are seven. Each class includes 30 shape samples. The sample category of this dataset is shown in Fig. 2. Each shape is matched against every other shape in the dataset. As there are 30 shapes in each category, up to 30 nearest neighbours are from the same category. We rate the performance based on the number of times the 30 nearest neighbours are in the same category.

The third dataset is available in [11] (see Fig. 3 for a subset of this shape dataset). The dataset has 70 classes of 2D shapes and every class has 20 shapes with different sizes and orientations. Therefore, there are 1400 shapes in this dataset in total. Each shape is matched against every other shape in the dataset. As there are 20 shapes in each category, up to 20 nearest neighbours are from the same category. We rate the performance based on the number of times the 20 nearest neighbours are in the same category.

Tables 2, 3 and 4 tabulate the correct recognition rates of the first 12/30/20 nearest neighbours in the same category for the first/second/third dataset. For the Zernike's moment, we used the 12^{th} order of moment features. For our proposed RS shape algorithm, we selected to use 79 invariant features. For RS moments, we also used 12^{th} order moments as the Zernike's moments. From Tables 2 and 3, it can be seen that our proposed algorithms compare favourably to the DTCWT moments and the Zernike's moments in terms of correct recognition rates. For Table 4, the DTCWT moments perform the best among the four methods compared in this paper. However, our proposed methods are both better than the Zernike's moments for this dataset. This demonstrates that our proposed methods in this paper are feasible in practical shape recognition.

We performed occlusion tests by removing 3 or 5 rows from the center of the shape images. Fig. 4 shows one original image and the occluded image. Table 5 tabulates the correct recognition rates of occlusion for the second shape dataset for the RS shape algorithm and the RS moments. It can be seen that the RS moments perform better than the RS shape algorithm for occlusions in these experiments. In general, the RS moments are better than the RS shape algorithm for occlusions.

We also conducted experiments for the noisy environment. We added Gaussian white noise with zero mean and standard deviation σ_n=10 or 20 to the original shape images (see Fig. 5). Table 6 tabulates the correct recognition rates of the two methods considered in this paper. It is clear that our proposed RS shape algorithm and the RS moments perform well in the noisy environment. In general, the RS shape algorithm is better than the RS moments for recognizing noisy shapes.

7. Conclusions

In this paper, we have studied the RS for image analysis, including moment invariants, invariant shape recognition and their noise robustness. Our classification algorithms are invariant to the translation, rotation, and scaling of the input shape

images. Experimental results have shown that the RS shape algorithm generates higher correct classification rates than the DTCWT moments and the Zernike's moments for the first and the second shape datasets. Our RS moments are comparable to the Zernike's moments and the DTCWT moments for the first shape dataset, but they are not as good as the Zernike's moments and the DTCWT moments for the second shape dataset. For the third dataset, the DTCWT moments perform the best among the four methods. However, our proposed RS shape algorithm and the RS moments are still better than the Zernike's moments in terms of correct classification rates. The RS are robust to occlusion and Gaussian white noise as well. Furthermore, the RS are fast because we can retrieve the RS basis functions saved in the file that was created before.

Given the fact that this is the first paper to apply the RS to moment invariants and shape recognition, more research needs to be done on these topics.

Acknowledgements

This work was supported by the research grants from the Natural Sciences and Engineering Research Council of Canada (NSERC).

References

1. A. Averbuch, R. R. Coifman, D. L. Donoho, M. Israeli, and Y. Shkolnisky. "A framework for discrete integral transformations I - the pseudo-polar Fourier transform," *SIAM Journal on Scientific Computing*, **30** (2008) 764–784.
2. G. Y. Chen and P. Bhattacharya, "Invariant pattern recognition using ridgelet packets and the Fourier transform," *International Journal of Wavelets, Multiresolution and Information Processing*, **7** (2009) 215–228.
3. G. Y. Chen and W. F. Xie, "Wavelet-based moment invariants for pattern recognition," *Optical Engineering*, *50* (2011).
4. J. Flusser, T. Suk and B. Zitova, Moments and Moment Invariants in Pattern Recognition, Wiley, 2009.
5. A. Khotanzad and Y. H. Hong, "Invariant image recognition by Zernike moments," *IEEE Transactions on Pattern Analysis and Machine Intelligence*, *12* (1990) 489–497.
6. L. T. Mainardi, L. Pattini and S. Cerutti, "Application of the Ramanujan Fourier transform for the analysis of secondary structure content in amino acid sequences," *Meth. Inf. Med.*, *46* (2007) 126–129.
7. L. T. Mainardi, M. Bertinelli and R. Sassi, "Analysis of T-wave alternans using the Ramanujan Sums," *Computer in Cardiology*, *35* (2008) 605–608.
8. M. Planat, "Ramanujan sums for signal processing of low frequency noise," *Phys. Rev. E.*, *66* (2002).
9. R. Ramanujan, "On certain trigonometric sums and their applications," *Trans. Cambridge Philos. Soc.*, **22** (1918) 259-276.
10. S. Samadi, M. O. Ahmad and M. N. S. Swamy, "Ramanujan sums and discrete Fourier transform," *IEEE Signal Processing Letters*, *12* (2005) 293–296.
11. Shape data for the MPEG-7 core experiment CE-Shape-1. http://www.cis.temple.edu/~latecki/TestData/mpeg7shapeB.tar.gz.
12. L. Sugavaneswaran, S. Xie, K. Umapathy and S. Krishnan, "Time-frequency analysis via Ramanujan sums," *IEEE Signal Processing Letters*, *19* (2012) 352–355.

13. N. Thakoor, J. Gao, S. Jung, "Hidden Markov Model-Based Weighted Likelihood Discriminant for 2-D Shape Classification," *IEEE Transactions on Image Processing*, **16** (2007) 2707–2719.

Table 1. The RS basis $c_q(n)$for q∈[1,20].

q																				
1	1																			
2	-1	1																		
3	-1	-1	2																	
4	0	-2	0	2																
5	-1	-1	-1	-1	4															
6	1	-1	-2	-1	1	2														
7	-1	-1	-1	-1	-1	-1	6													
8	0	0	0	-4	0	0	0	4												
9	0	0	-3	0	0	-3	0	0	6											
10	1	-1	1	-1	-4	-1	1	-1	1	4										
11	-1	-1	-1	-1	-1	-1	-1	-1	-1	-1	10									
12	0	2	0	-2	0	-4	0	-2	0	2	0	4								
13	-1	-1	-1	-1	-1	-1	-1	-1	-1	-1	-1	-1	12							
14	1	-1	1	-1	1	-1	-6	-1	1	-1	1	-1	1	6						
15	1	1	-2	1	-4	-2	1	1	-2	-4	1	-2	1	1	8					
16	0	0	0	0	0	0	0	-8	0	0	0	0	0	0	0	8				
17	-1	-1	-1	-1	-1	-1	-1	-1	-1	-1	-1	-1	-1	-1	-1	-1	16			
18	0	0	3	0	0	-3	0	0	-6	0	0	-3	0	0	3	0	0	6		
19	-1	-1	-1	-1	-1	-1	-1	-1	-1	-1	-1	-1	-1	-1	-1	-1	-1	-1	18	
20	0	2	0	-2	0	2	0	-2	0	-8	0	-2	0	2	0	-2	0	2	0	8

Table 2. The correct recognition rates (%) of the proposed RS shape algorithm, the RS moments, the DTCWT moments, and the Zernike's moments for the first shape dataset. The highest recognition rates are highlighted in bold font.

RS Shape Algorithm					
100	**95.37**	**92.59**	**91.67**	81.48	**83.33**
82.87	**79.17**	**73.61**	65.74	63.43	56.02
RS Moments					
100	93.52	85.19	80.56	81.48	79.63
77.31	70.83	68.98	**67.13**	**64.35**	**64.35**
DTCWT Moments					
100	94.44	88.89	82.41	80.56	73.61
72.22	68.52	67.59	61.11	52.78	48.15
Zernike's Moments					
100	94.44	91.67	87.96	**85.65**	81.02
74.07	75.46	66.67	66.20	50.00	51.85

Table 3. The correct recognition rates (%) of the proposed RS Shape Algorithm, the RS moments, the DTCWT moments, and the Zernike's moments for the second shape dataset. The highest recognition rates are highlighted in bold font.

RS Shape Algorithm					
100	**100**	**100**	**100**	**100**	**100**
100	**100**	**100**	**100**	**100**	**100**
100	**100**	**100**	**100**	**100**	**100**
100	**100**	**100**	**99.52**	**100**	**100**
99.52	**100**	**100**	**100**	**98.57**	**95.24**
RS Moments					
100	99.52	98.57	99.05	99.05	99.05
96.67	96.67	96.67	92.86	93.33	93.33
86.19	84.76	76.67	69.05	67.14	67.14
68.10	70.48	65.71	64.29	62.38	57.14
55.24	46.19	52.38	51.43	40.95	44.76
DTCWT Moments					
100	100	100	100	100	100
100	100	100	100	100	100
99.52	99.05	100	100	100	100
99.52	100	100	99.52	99.05	100
99.52	99.05	99.05	98.10	89.52	75.71
Zernike's Moments					
100	100	99.52	100	100	100
100	100	99.52	99.52	100	99.05
100	98.57	98.57	99.52	99.05	100
99.05	99.05	98.57	99.05	99.52	98.09
98.09	99.05	99.52	96.67	93.33	79.52

Table 4. The correct recognition rates (%) of the proposed RS shape algorithm, the RS moments, the DTCWT moments, and the Zernike's moments for the third shape dataset. The highest recognition rates are highlighted in bold font.

RS Shape Algorithm				
100	88.50	79.21	72.57	61.57
60.79	56.36	54.00	48.79	47.29
43.07	40.71	38.64	35.50	33.00
29.86	31.43	25.07	28.07	24.21
RS Moments				
100	89.86	79.50	74.21	65.43
61.86	58.57	57.14	53.36	50.21
47.86	**45.71**	**45.64**	**40.43**	**38.71**
33.64	32.29	**31.07**	27.86	25.14
DTCWT Moments				
100	**90.93**	**82.14**	**77.21**	**69.64**
65.29	**60.86**	**57.93**	**55.00**	**51.64**
48.00	44.71	41.93	39.29	37.07
36.57	**34.64**	29.93	**30.71**	**27.29**
Zernike's Moments				
100	84.00	74.14	67.43	58.79
53.57	48.07	45.57	40.93	39.21
35.86	36.29	34.21	32.07	29.86
27.71	26.71	23.93	23.71	21.21

Table 5. The correct recognition rates (%) of the proposed RS Shape algorithm and the RS moments for the second shape dataset. Every shape image is distorted by removing T=3 or 5 rows of pixels from the center of the original shape.

RS Shape Algorithm (T=3)					
67.62	67.15	66.19	65.71	65.71	65.71
66.19	65.71	64.76	65.71	66.67	66.19
67.14	69.05	66.19	64.76	68.57	65.71
64.76	64.29	65.71	63.33	59.52	63.81
62.86	60.48	61.43	62.38	58.57	48.57
RS Shape Algorithm (T=5)					
42.86	42.38	34.76	37.62	36.19	35.71
34.29	35.24	34.76	34.29	34.29	36.67
35.71	33.33	37.62	34.29	36.19	31.43
37.14	32.86	36.67	31.90	31.90	34.76
30.95	36.19	31.43	31.43	30.48	29.05
RS Moments (T=3)					
100	99.05	98.10	98.57	99.52	97.14
95.71	95.71	95.71	96.19	92.86	91.90
90.00	84.76	81.43	74.76	78.57	75.71
70.95	69.05	69.05	63.81	62.38	59.52
59.52	58.10	51.90	52.38	38.57	39.52
RS Moments (T=5)					
100	94.76	95.24	93.81	93.33	92.38
93.33	92.38	88.57	88.57	87.62	86.19
87.62	82.38	77.14	75.24	73.81	74.29
70.00	66.19	68.10	64.29	63.33	57.14
61.90	52.86	48.57	46.19	40.48	31.90

Table 6. The correct recognition rates (%) of the proposed RS Shape Algorithm and the RS moments for the second shape dataset. Every shape image is distorted by adding Gaussian white noise to the shape image with zero mean and standard deviation σ_n=10 or 20.

RS Shape Algorithm (σ_n=10)					
100	100	100	100	100	100
100	100	100	100	100	99.52
100	100	100	100	99.52	100
99.52	99.52	99.52	99.52	100	99.52
99.52	99.52	100	99.52	99.52	88.57
RS Shape Algorithm (σ_n=20)					
98.57	97.62	99.05	97.62	97.14	98.09
99.05	98.10	98.57	97.62	98.10	97.62
99.05	98.57	98.57	96.67	97.62	97.62
99.05	97.62	97.62	97.14	97.14	97.14
98.10	93.81	95.24	90.95	81.43	78.10
RS Moments (σ_n=10)					
100	99.52	99.05	99.05	99.05	98.10
97.62	97.14	93.81	93.81	92.86	92.86
87.14	81.90	74.29	68.57	71.43	63.33
71.43	71.43	66.67	64.76	62.86	53.81
50.95	51.43	53.33	47.14	48.57	42.38
RS Moments (σ_n=20)					
100	99.52	99.05	99.52	97.62	97.62
98.57	94.76	93.81	94.29	93.81	89.05
84.29	83.81	73.33	70.00	68.57	67.14
67.62	69.52	64.29	66.19	62.86	59.05
55.24	51.43	50.48	47.62	48.57	47.62

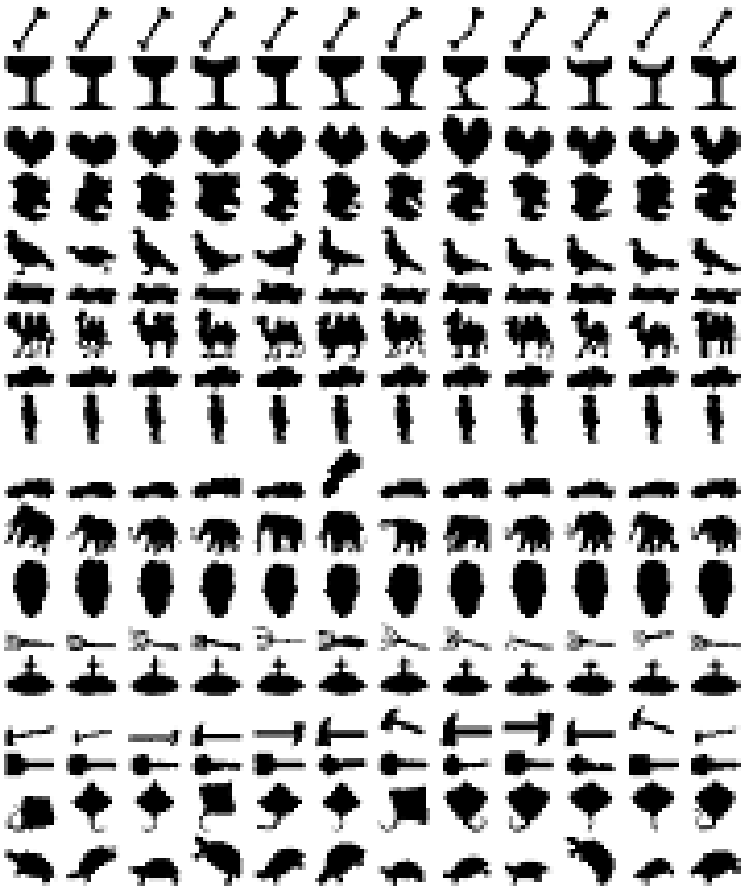

Fig. 1. The samples of the first shape dataset.

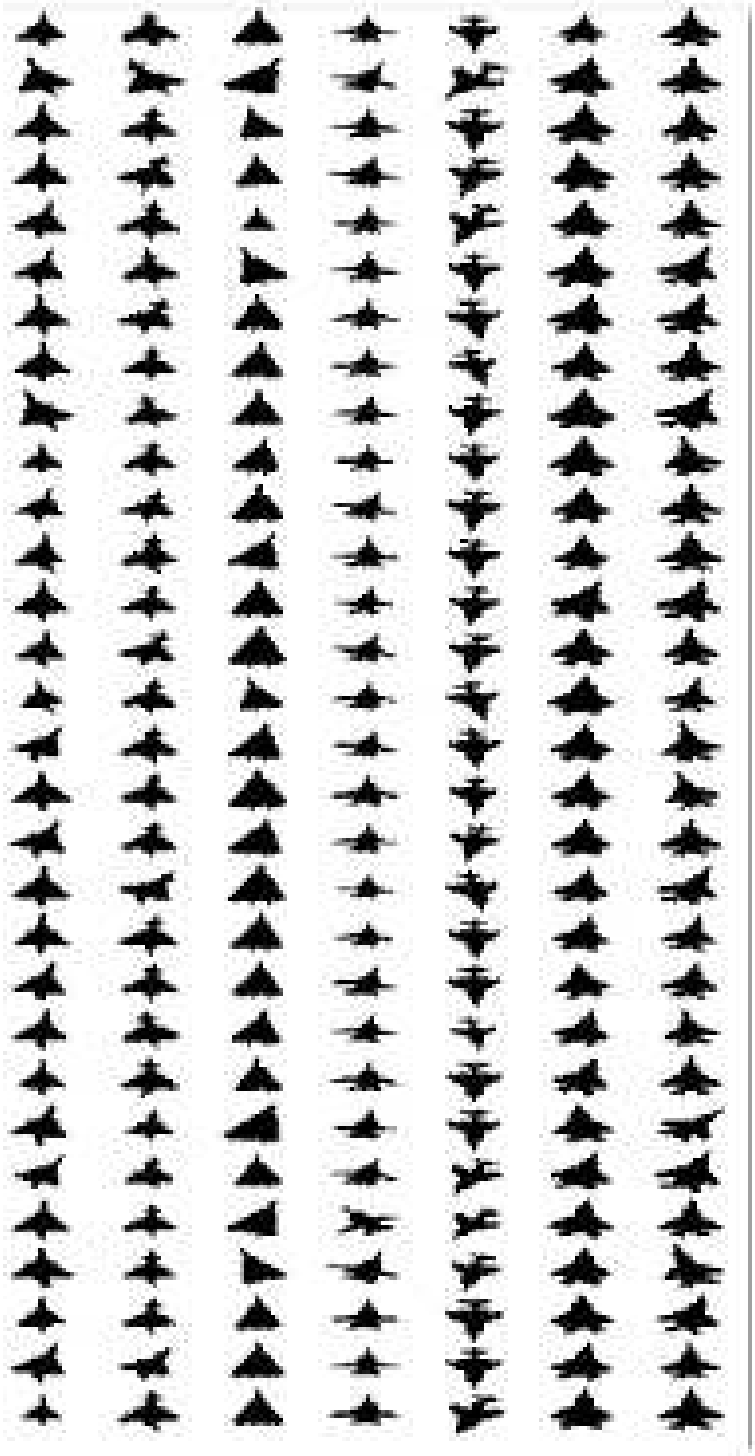

Fig. 2. The samples of the second shape dataset.

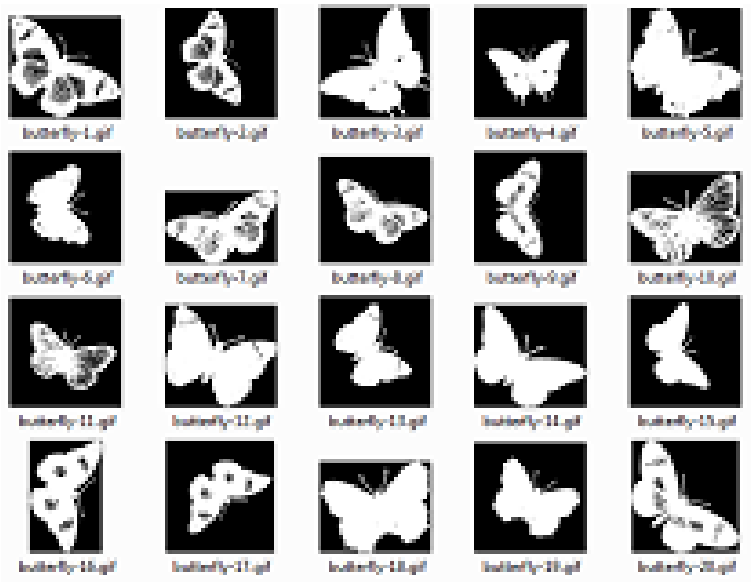

Fig. 3. The samples of the third shape dataset.

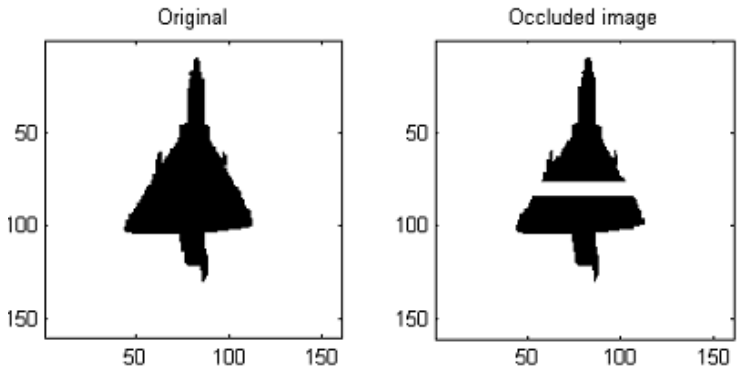

Fig. 4. A shape image and its occluded image by removing five lines of pixels at the center of the image.

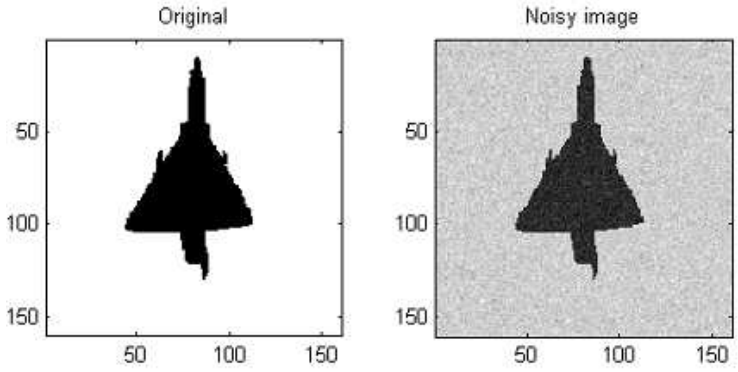

Fig. 5. A shape image and its noisy version by adding Gaussian white noise with zero mean and standard deviation σ_n=20.